Article:
Al-Asadi, MT, Al-damook, A and Wilson, MCT (2018) Assessment of vortex generator shapes and pin fin perforations for enhancing water-based heat sink performance. International Communications in Heat and Mass Transfer, 91. pp. 1-10. ISSN: 0735-1933

https://doi.org/10.1016/j.icheatmasstransfer.2017.11.002

Assessment of vortex generator shapes and pin fin perforations for enhancing water-based heat sink performance

Mushtaq T. Al-Asadi*[a, b], Amer. Al-damook[c], M. C. T. Wilson[a]

[a]*Institute of Thermofluids, School of Mechanical Engineering, University of Leeds, UK*
[b]*Refrigeration Department, Eng. Division, South Oil Company, Ministry of Oil, Basrah, Iraq.*
[c]*Mechanical Engineering Department, University of Anbar, MOHESR, Iraq*

Abstract

In this study, two models have been analysed numerically to examine the impact of the geometry and the working fluid under laminar flow on heat and flow characteristics. The first model is a perforated pinned heat sink (PPHS) and the second is a new design of a uniform micro-channel having different shapes of vortex generators (VGs) positioned at intervals along the base of the channel. The VG shapes are circular, triangular and rectangular, and are compared to each other based on constant volume. Models with Reynolds number in the range of 50 to 2300 are subjected to a uniform heat flux relevant to microelectronics air and water cooling. Validations against previous micro-channel studies were conducted using the COMSOL Multiphysics® software package and found to be in good agreement. The results show that there is no significant enhancement in heat transfer using water in PPFHS. However, the VGs described here are shown to offer significant potential in combatting the challenges of heat transfer in the technological drive toward lower weight/smaller volume electrical and electronic devices. It is also found that the circular VGs offer the best heat performance among the proposed shapes.

Keywords: vortex generators, micro-channel, micro scale cooling system, heat transfer enhancement, water vs air efficiency.

---

*Corresponding author:

Email: ml13mtka@leeds.ac.uk;

Nomenclature

A_s	surface area of the whole heat sink (μm^2)
C_p	Specific heat, J/kg.K
D_h	Hydraulic diameter, μm
k	Thermal conductivity, W/m.K
L	Channel length, μm
p	Pressure, N/m^2
PFHS	Plate-fin heat sink
PHS	Pinned heat sink
q	Uniform heat flux, W/cm^2
Re	Reynolds number
T	Temperature, K
u,v,w	Velocity components
u_{in}	Inlet velocity
VG	Vortex generator
x	Axial distance, μm

Greek Symbols

μ	Viscosity, kg/ms
θ	Thermal resistance, K/W
ρ	Density, kg/m^3

Subscripts

ave	average
In	inlet
L	liquid
Out	outlet
S	solid

1. Introduction

Since 1931, researchers have explored ways of managing the heat flux generated from electrical devices and offering better heat transfer rates using different types of heat sink cooling systems. One of the most popular heat sinks used in air-cooled systems is a plate-fin heat sink (PFHS) because of its simplicity to manufacture. Many investigations of PFHSs have studied and optimized the fins' height, thickness and separation, yielding predictions of heat transfer and entropy [1-4]. Other designs such as pinned heat sinks (PHSs) have also been considered in both inline and staggered arrangements [5] to enhance the heat transfer rate. They can take several shapes such as rectangular, square, circular, elliptical, NACA and drop form [6-8].

Continuing developments in electronic and electrical devices, and the increased heat density associated with miniaturisation, mean that thermal management of high heat fluxes remains an active area of research [9]. One approach is to improve the thermo-physical properties of the coolants, for example by developing nanofluids [10, 11]. Alternatively, the geometry of the heat sinks can be adapted to improve heat transfer, for example by modifying the pins in PHSs or the channels in PFHSs. One very successful approach is the use of micro-channels. Micro-channels first appeared in 1981 [12] and have been classified in terms of their hydraulic diameters, D_h, [13-15] and distinguished from conventional channels. Using micro-channels can enhance the thermal performance of cooling systems [16] while shrinking their size and weight [17].

Indeed, developments in manufacturing capabilities and processes have opened wide possibilities for modifying the heat sinks types to enhance the performance of cooling systems. Therefore, Al-Damook et al. [18] examined a modified perforated PHS numerically and experimentally with turbulent air as the working fluid. The results showed that the heat transfer rate enhanced and, at the same time, the pressure penalty and fan power decreased using perforated pin fins compared to solid pin fins.

Many experimental and numerical studies have investigated the heat transfer and fluid flow performance of various modified geometries such as micro-channels having grooves and ribs [19-22]. One of the effective modified micro-channel types is a uniform channel having vortex generators (VGs). The enhancement of heat transfer and fluid flow characteristics were investigated experimentally in 1969 [23]. VGs can take various forms such as protrusions, wings, inclined blocks, winglets, fins, and ribs [24, 25], and have been used to enhance heat transfer in different geometries such as circular and non-circular ducts under turbulent flow [26-29]. They have also been used in laminar flow [24, 30-33] which is effective to enhance the heat transfer rate, with flat plate-fins in rectangular channels [34-36], tube heat exchangers [17, 37], heat sinks [30, 38] and rectangular narrow channels [32, 39].

Among different types of micro channel shapes, the rectangular micro-channel was the best geometry based on the numerical investigation of Xia et al. [40], who considered various microchannel shapes. They also investigated the distribution of flow through a collection of 30 micro-channels forming a heat sink, considering different header chamber shapes and inlet/outlet positions.

Recently, research has focused on VGs located on the channel sidewalls of the geometry. For example, Chia et al. [41] studied numerically the influence of fan-shaped ribs on the sidewalls of a silicon micro-channel with water in laminar flow. The results indicate that using fan-shaped ribs in the micro-channel can decrease the thermal resistance by up to 40% compared to a smooth channel. Furthermore, another study by Chia et al. [42] investigated the effect of five shapes of sidewall ribs in comparison to the performance of a smooth micro-channel using water in laminar flow. The rib cross-sections were rectangular, forward triangular, backward triangular, equal side triangular and semi-circular, and the results showed that the heat transfer rate was enhanced while the pressure penalty increased compare to the smooth channel. Also, it was found that the circular ribs offered the best thermal performance among VG models.

A 2D numerical study by Cheraghi et al. [16] considered a smooth channel, with fixed heat flux applied to the wall sides, having an adiabatic cylinder inside which was perpendicular to the laminar flow direction with a Reynolds number of 100 and Prandtl number ranging from 0.1 to 1. They investigated the influence of the position of the cylinder and found that the maximum enhancement occurred when the cylinder was fixed halfway from the base to the top of the channel. Also, the results showed that the low Prandtl number had a positive effect on heat transfer enhancement.

Furthermore, a modified channel having cylindrical vortex generators inside a uniform channel using turbulent flow with a Reynolds number of 3745 has been investigated numerically [43]. It was found that using a cylindrical vortex generator enhanced the heat transfer by 1.18 times compared to the uniform channel.

In addition, a recent investigation by Al-asadi et al. [44] studied the influence of cylindrical VGs with radii up to 400 μm on heat transfer and pressure drop characteristics under laminar flow conditions. Quarter- and half-circular VGs on the base of the micro-channel were considered with a constant heat flux ranging from 100 to 300 W/cm^2 and Reynolds number up to 2300. The results showed that heat transfer was enhanced using half-circular VGs, whereas the quarter-circle VGs offered no improvement. The results also indicated that the heat transfer was further enhanced when a gap was introduced between each channel wall and the ends of the VGs.

Beyond the ideas examined in the previous work mentioned above, there remains great scope for further exploration of geometry-based enhancement of heat sink performance with water as the working fluid. This paper therefore investigates two different geometries. The first is a

perforated pinned heat sink (PPHS). As indicated above, this heat sink was developed for an air-cooled system, and the key question here is whether or not the same kind of modification will be beneficial with water instead of air as the coolant. The second geometry combines recent ideas from the literature and is a micro-channel with different configurations of VGs including rectangular, square, forward triangular and backward triangular located on the channel base. The influence of the water on conjugate heat transfer is explored under laminar flow conditions. Such configurations are relevant to the cooling of electronic devices like chips used in computers and datacentres.

The computational method is described in the second section of the paper, after which section 3 describes the validation and mesh sensitivity and section 4 discusses the numerical results. The conclusions of the study are drawn in section 5.

2. Computational method

2.1 Geometry description and computational domain

Two models of heat sinks are examined using water in laminar flow. The first is a perforated PHS adopted from Al-Damook et al. [18] as shown in Fig. 1 (a and b). The thermal performance of this model is examined using water in laminar flow (instead of the air for which the system was originally developed). The second configuration is a micro-channel adopted from Al-asadi et al. [44] as shown in Fig 2a. The computational domain consists of a single micro-channel with rectangular cross-section, with appropriate symmetry planes to represent the whole heat sink. The total base area of the heat sink is taken as $A_s = 6.27\times10^8$ μm^2. The dimensions of the single micro-channel are shown in Fig. 2b and Table 1. The new shapes of the VGs, such as rectangular, square, forward triangular and backward triangular, are seen in Fig. 3 (a-e). The key factor in examining the influence of different shapes on heat and flow performance is the constant volume of 0.0314 mm^3 for each VG as illustrated in Table 1.

2.2 Conjugate heat transfer model

The water flow in the micro-channel is considered as a laminar flow, steady state, weakly compressible and Newtonian, with gravitational and viscous dissipation effects neglected. With $\boldsymbol{u} = (u, v, w)$ representing the liquid velocity in (x, y, z) Cartesian coordinates, and p, ρ and μ denoting the liquid pressure, density and viscosity respectively, the (dimensional) governing equations for the flow are the usual continuity and Navier-Stokes equations:

$$\nabla \cdot (\rho \boldsymbol{u}) = 0 \tag{1}$$

$$\rho(T_L)(\boldsymbol{u} \cdot \nabla)\boldsymbol{u} = \nabla \cdot \left[-p\boldsymbol{I} + \mu(T_L)(\nabla \boldsymbol{u} + (\nabla \boldsymbol{u})^T) - \frac{2}{3}\mu(T_L)(\nabla \cdot \boldsymbol{u})\boldsymbol{I}\right]. \tag{2}$$

The energy equation for the liquid phase in the micro-channel is:

$$\rho C_p \boldsymbol{u} \cdot \nabla T_L = \nabla \cdot (k \nabla T_L) \tag{3}$$

where, C_p, T_L, and k are respectively the specific heat, temperature, and thermal conductivity of the liquid, with temperature dependence defined as follows:

$$\rho(T_L) = 838.466135 + 1.40050603T_L - 0.0030112376T_L^2 + 3.71822313 \times 10^{-7}T_L^3 \tag{3a}$$

$$\mu(T_L) = 1.3799566804 - 0.021224019151T_L + 1.3604562827 \times 10^{-4}T_L^2 - 4.6454090319 \times 10^{-7}T_L^3 + 8.9042735735 \times 10^{-10}T_L^4 - 9.0790692686 \times 10^{-13}T_L^5 + 3.8457331488 \times 10^{-16}T_L^6 \tag{3b}$$

$$C_p(T_L) = 12010.1471 - 80.4072879T_L + 0.309866854T_L^2 - 5.38186884 \times 10^{-4}T_L^3 + 3.62536437 \times 10^{-7}T_L^4 \tag{3c}$$

$$k(T_L) = -0.869083936 + 0.00894880345T_L - 1.58366345 \times 10^{-5}T_L^2 + 7.97543259 \times 10^{-9}T_L^3 \tag{3d}$$

Conduction in the solid is captured by:

$$\nabla \cdot (k_S \nabla T_S) = 0 \tag{4}$$

where T_S and k_S are respectively the temperature and thermal conductivity of the solid Aluminium.

2.3 Boundary conditions

For both configurations, PPHS and VG shapes, symmetry conditions were applied at the left- and right-hand outer boundaries of the domain, while a uniform heat flux was applied at the bottom boundary. The top boundary was considered as adiabatic. At the inlet, the velocity of the flow, u_{in}, was set to achieve a specified Reynolds number,

$$Re = \frac{\rho u_{in} D_h}{\mu}, \tag{5}$$

and the inlet temperature was fixed at 293.15 K. At the outlet, the pressure was set to zero, and on the micro-channel walls, the no-slip condition was applied. The boundary conditions are also illustrated in Table 2.

2.4 Solver Settings and data acquisition

The grid is adopted from Al-asadi et al. [44] to improve the quality of the numerical prediction near curved and sharp rib surfaces. A commercial finite element method-based code, COMSOL Multiphysics® v. 5.2a is used to solve the fully coupled continuity, momentum and energy equations iteratively. The procedure continues until the norm of the residuals of the governing equations is less than 10^{-3}.

The heat transfer performance is evaluated via the thermal resistance, which is commonly defined in one of two ways in terms of temperature differences. The first is $\Delta T = T_{max} - T_{in}$ [6, 45] , the second is $\Delta T = T_{ave} - T_{in}$ [44, 46] which is considered in this study, hence

$$\Theta = \frac{T_{ave} - T_{in}}{A_s\, q} \tag{6}$$

where T_{ave} is the average temperature of the base, T_{in} is the inlet temperature, and q is the heat flux through the base of the heat sink.

To examine the overall heat transfer performance while considering the pressure penalty, a thermal-hydraulic performance evaluation criteria (PEC) index [19, 20] is used. The PEC index is defined in terms of directly computed quantities, namely the thermal conductance of the system (i.e. the reciprocal of the thermal resistance) and the actual pressure drop. Hence the PEC index is defined as:

$$\mathrm{PEC} = \frac{\theta_s/\theta}{(\Delta P/\Delta P_s)^{1/3}} \tag{7}$$

where ΔP and θ are the pressure drop and thermal resistance in a microchannel containing VGs and ΔP_s and θ_s are the same quantities in the corresponding uniform micro-channel.

3. Validation and grid independence test with previous studies

The mesh sensitivity analysis and the code validation for both heat sink models were adopted from Al-Damook et al. [18] for PHSs; and Al-asadi et al. [44] for the VG models. Furthermore, the present model was also compared to previous numerical and experimental studies. The first study was an experimental investigation of a straight micro-channel done by Kawano et al. [47]. The second validation was against numerical study presented by Qu and Mudawar [48]. Both studies used the same material (silicon) and the height, width and length of the micro-channel were 180 µm, 57 µm, 10 mm respectively. The top of micro-channel was subjected to a uniform heat flux of 90W, while the side walls were set to be symmetry, and the bottom wall was adiabatic. Laminar flow was used in the studies, with Reynolds number ranging from 80 to 400. To validate the present computational method, the same system was modelled and the resulting calculations of the thermal resistance (calculated in this instance as $R_{th,\,out} = (T_{surface,\,Max} - T_{fluid,\,in})/q$) are shown in Fig. 4. As can be seen, excellent agreement with the experiments is found.

4. Results and discussions

In this study, the results will be divided into two parts. The first part examines the influence of the geometry of Al-Damook et al. [18] with water instead of air as a working fluid. The second part presents the impact of using various VGs shapes (See Fig. 3) on heat transfer and fluid flow characteristics.

Three-dimensional laminar flow simulations were conducted with Reynolds number in the range 50-2300 and heat flux ranging from 75 to 100 W/cm^2 to examine the impact of the vortex generators on the conjugate heat transfer, with water as the coolant. The results show that the thermal resistance decreased as the Reynolds number increased due to the increase of the velocity which leads to an enhanced heat transfer rate, however, as to be expected, the pressure drop increased.

The results presented below focus on the particular value of 100 W/cm^2 for the heat flux, because the system using water can achieve temperature reduction for such high heat fluxes. However, higher heat fluxes are not considered due to the upper temperature limit for operation of electronic devices [45, 49, 50].

4.1 Perforated PHS using water

The perforated PHS model is compared with the solid PHS to examine the influence of using water on hydraulic and thermal performance. Fig. 5(a) presents numerical predictions of the pressure drop through the PHS. It is found that there is no significant decrease in pressure drop when using the perforated model compare to the solid one. Fig. 5(b) describes the average temperature of PHS base plate, T_{case}, as a function of the Reynolds number in the range of $300 \leq Re \leq 1100$ for both solid and perforated pinned heat sinks. Both sets of data approximately show the consistent trend of the same CPU temperatures. This is because the viscosity and the thermal capacity of water are higher than those of air and the perforations diameter may be not large enough to pass water through them easily. This leads to the conclusion that the heat sink perforations do not reduce either the pressure drop or CPU temperature. Therefore, there is no benefit in using PPHS with water as a coolant. It is clear that replacing the working fluid (air) by water using perforation technique does not offer significant enhancement in heat transfer and pressure drop, therefore, the focus below will be on the VGs of different shapes (see Fig. 3) using water as a coolant and exploring their effect on heat and flow characteristics.

4.2 VGs shape influence

The proposed VG shapes are compared to a uniform channel. The key factor in this comparison is that all VG configurations are considered to have an equal volume of 0.0314 mm^3. The heat transfer performance and fluid flow effects were examined using laminar flow and a constant heat flux ranging from 75 to100 W/cm^2 and Reynolds number in the range of 50 to 2300. Before investigating the influence of different VG configurations on heat transfer and fluid flow, Fig. 6a shows the effect of heat flux on thermal resistance. As to be expected, the thermal resistance increases with increasing heat flux for the given Reynolds number. However, using water as a

coolant can enhance heat transfer rate for high heat flux. Therefore, 100 W/cm^2 is considered in the following results. Furthermore, in particular applications there is a temperature limitation in operating electronic chips, as calculated results showed that the working temperature of 356 K is suitable for the experimental applications, which can be achieved using Re of 300. In addition, Fig 6a also presents that at high Reynolds number (2000-2300) there is no significant improvement in thermal resistance. Hence, the later results are presented at Reynolds number in the range of 300-2000. Another important factor in heat transfer studies is the pressure drop, since it is directly related to the power consumption and hence the overall cost of the system for a long period of operation. Fig. 6b reveals that the pressure drop is higher at low heat flux, and this is due to the viscosity effect as the viscosity of colder water is higher, and hence a larger pressure gradient is required to drive the flow at a given speed. Thus Fig. 6b shows that no significant effect is found in changing heat flux from 75 to 100 W/cm^2. The detail of the effects of VG shapes on conjugate heat transfer are presented in different sections below.

4.2.1Triangular shapes

A uniform channel is taken as a reference adopted from Al-asadi et al. [44] to be compared to the three new VG configurations of triangular shape which are forward (T) backward (T1) and symmetric (T3) (See Fig. 3). As discussed in the previous section (4.2), the heat flux is taken as 100 W/cm^2 and Reynolds number is ranging from 300 to 2000 to assess the impact of thermal resistance and pressure drop as shown in Fig. 7a and b. The influence of triangular VG shapes on thermal resistance is presented in Fig. 7a, where it is found that the symmetric (T3) VG model offers the lowest thermal resistance, followed by forward (T), then the backward (T1), while the highest thermal resistance is for the uniform channel. This is also seen in Fig. 8a (temperature contours) which shows that the T3 VG model at Re = 800 offers the lowest temperature. This is because of the VG configuration related to the fluid flow. For instance, there is a stagnant zone before the VGs of model T1 because the flow encounters a vertical face (See Fig. 8b), which generates a hot spot, while this effect is smaller for the T and T3 models due to the inclined upstream surface of the VG. However, the T3 model has smaller stagnant zone compared to T and T1 models, this can be seen in Fig 8b. It is clear that all triangular configurations offer heat transfer enhancement compared to the uniform channel. However, the price paid is a significantly higher pressure drop compared to the uniform channel, as shown in Fig 7b. The next section presents the influence of rectangular VGs models on conjugate heat transfer.

4.2.2 Rectangular shapes

In this section, various shapes of rectangular configuration (see Fig. 3d-f) are compared to the uniform channel to examine their effect on thermal resistance and pressure drop. Fig. 9a shows

the effect of rectangular VGs in various models (Vertical rectangular (R1), Horizontal rectangular (R2) and Square (S)) on thermal resistance. It is found that the S VG shape offers the lowest thermal resistance compared to R1, R2 and the uniform channel especially at Re more than 900, while model R1 offers the best thermal resistance at Re less 800. The reason behind that can be explained using Fig. 10 a and b. Fig. 10a shows that the S model has lowest temperature (K) because its dimensions make a balance between the height of the VGs which act as fins in terms of heat transfer and the stagnant zone behind the VGs in terms of fluid. It can be seen that the effect of heat transfer is more than the effect of the fluid flow in the case of comparing R1 and S models. Therefore, the R1 model offers a better heat transfer rate compared to the S model at low Re (See Fig. 9a). This can be discussed in more detail through association with the fluid flow contours shown in Fig 10b, which shows that the height of S model lies between R1 and R2. Obviously generating a hot spot behind each VGs depends on the stagnant zone that also depends on the VG's height. For example, Fig. 10b shows that the S model has a larger stagnant area than R2 model, but the S model still has the lowest thermal resistance (see Fig. 9a). This can be attributed to the fact the fast stream (blue stream) passing over the S model is more than the one passing over the R2 model (See Fig. 10b). Interestingly, the S model also offers the lowest pressure drop compared to R1 and R2 models as shown in Fig. 9b, this is due to the height (h) of the VGs facing the water (see Table 1).

4.2.3 Circular shapes

Circular (C) VGs shown in Fig. 3g with the dimensions presented in Table 1 are compared to the uniform channel to study the shape effect on the conjugate heat transfer. Fig. 11a reveals that the thermal resistance decreased significantly using circular VGs compared to the uniform channel. However, the pressure drop of C model is higher than the uniform channel due to the VGs which constrict and disturb the water in the micro channel as shown in Fig. 11 b. The temperature contours (in K) of the circular VGs are compared to the uniform channel in Fig. 12a which reveals how the circular VGs assist in enhancing the heat transfer by dissipating the heat from the base of the channel to the water. VGs help to develop the secondary flow by disturbing the flow (mixing the cold and hot fluids) which leads to reducing the boundary layer as shown in Fig. 12b.

4.2.4 Comparison of the VGs shapes

The sections above compared different VGs to the uniform channel for both thermal resistance and pressure drop. Overall, all proposed models enhanced the thermal resistance compared to the uniform channel, but all of them have higher pressure drop than the uniform channel. Hence, it is natural to ask what configuration is the best in terms of heat transfer and pressure drop. Therefore, Fig. 13a presents the lowest thermal resistance of each group of VGs shapes. It is found that the circular VG shape has the lowest thermal resistance compared to S and T3

models. In addition, Fig .13b shows that the C model also has a lower pressure drop than T3 and S models, but still much higher than the uniform channel. VGs enhance the heat transfer, but this enhancement depends on the reduction of the hot spot area behind the VGs. For instance, the hot spot behind the C model is less than for the T3 and S models. Therefore, the C model has the lowest thermal resistance as shown in Fig. 14a. This can be attributed to the fact that the main flow passes over the VGs and deflects it, generating a recirculation, which may act to reduce the thermal boundary layer and enhance the heat transfer by mixing hot and cold liquid [42, 51] as clearly presented in Fig. 14b.

4.3 Hydraulic thermal performance

The criterion used in this section is based on comparison of the heat transfer enhancement and the pressure drop increment relative to the behaviour of a uniform channel (see eq. 7). Fig. 15 shows the PEC for the best models in terms of thermal resistance (T3, S and C models, sec. 4.2.4). The results indicate that the lowest PEC is for T3 model, then S model, as the highest PEC is for C model. This can be attributed to how PEC is applied (see eq.7) to evaluate the overall heat transfer, for example, C model has the lowest thermal resistance and pressure drop compared to VG models (See Fig. 13 and 14). Therefore, the C model has the highest PEC compared to the other VG models. However, C model still below 1 (PEC for the uniform channel).

5. Conclusions

In this study, two main models are studied to examine the impact of the geometry and the fluid type on heat transfer and fluid flow characteristics. A perforated pinned heat sink is the first part, while the second part is the vortex generators (VGs) of different shape, namely Forward triangular (T1), Backward triangular (T), Symmetric triangular (T3), Vertical rectangular (R1), Horizontal rectangular (R2), Square (S) and Half-circle (C). Both models have been investigated under laminar flow ($50 \leq Re \leq 2300$) subjected to a uniform heat flux related to CPUs in electronic devices ranging from 75 to 100 W/cm^2. The aim of this study is to suggest a new geometry which meets the rapid developments of the electronic devices. Therefore, the outcomes out of this research are summarised in the following points.

- It does not necessarily follow that a geometrical modification that improves heat transfer for one fluid will also enhance performance for a different working fluid. In the present study, the perforated pinned heat sink that is effective with air showed insignificant enhancement in heat transfer rate or reduction in pressure drop compared to the solid pins when water is the coolant.
- For triangular VG configurations (Forward triangular (T1), backward triangular (T) and (c) Symmetric triangular (T3))**.** (T, T1 and T3) it is found that the lowest thermal resistance is T3 model, while the lowest pressure drop is T model.
- For the rectangular VG models (Vertical rectangular (R1), horizontal rectangular (R2) and Square (S)), the results show that S model offers lowest thermal resistance and pressure drop compared to R1 and R2, but S model still higher pressure drop than the uniform channel.
- All proposed VG models offer a significant heat transfer performance while, as to be expected, the price paid is the additional pumping power needed to drive the flow compared to the uniform channel.
- Circular VGs offer the lowest thermal resistance, followed by rectangular and triangular VGs. However, the pressure drops of all proposed VGs models are much higher than the uniform channel.
- Thermal hydraulic performance (PEC) is used to evaluate the combination of heat transfer and the pressure drop of the system and come out with an overall evaluation. It is found that the circular VG model offered the highest PEC (PEC≈ 0.95) in comparison to triangular and square configurations, but still below the 'neutral' value of PEC = 1.

6. References

1. Knight, R.W., J.S. Goodling, and D.J. Hall, *Optimal Thermal Design of Forced Convection Heat Sinks-Analytical.* Journal of Electronic Packaging, 1991. **113**(3): p. 313-321.
2. Knight, R.W., J.S. Goodling, and B.E. Gross. *Optimal thermal design of air cooled forced convection finned heat sinks-experimental verification*. in *Thermal Phenomena in Electronic Systems, 1992. I-THERM III, InterSociety Conference on*. 1992.
3. TEERTSTRA, P., M.M. YOVANOVICH, and J.R. CULHAM, *ANALYTICAL FORCED CONVECTION MODELING OF PLATE FIN HEAT SINKS.* Journal of Electronics Manufacturing, 2000. **10**(04): p. 253-261.

4. Copeland, D. *Optimization of parallel plate heatsinks for forced convection*. in *Semiconductor Thermal Measurement and Management Symposium, 2000. Sixteenth Annual IEEE*. 2000.

5. Sparrow, E.M., J.W. Ramsey, and C.A.C. Altemani, *Experiments on In-line Pin Fin Arrays and Performance Comparisons with Staggered Arrays.* Journal of Heat Transfer, 1980. **102**(1): p. 44-50.

6. Zhou, F. and I. Catton, *Numerical Evaluation of Flow and Heat Transfer in Plate-Pin Fin Heat Sinks with Various Pin Cross-Sections.* Numerical Heat Transfer, Part A: Applications, 2011. **60**(2): p. 107-128.

7. Jacobs, E.N., *Tests of six symmetrical airfoils in the variable density wind tunnel.* 1931.

8. Jacobs, E.N., K.E. Ward, and R.M. Pinkerton, *The characteristics of 78 related airfoil sections from tests in the variable-density wind tunnel.* 1933.

9. Li, H.-Y., et al., *Enhancing heat transfer in a plate-fin heat sink using delta winglet vortex generators.* International Journal of Heat and Mass Transfer, 2013. **67**(0): p. 666-677.

10. Al-Asadi, M.T., et al., *Heat Transfer Enhancements Using Traditional Fluids and Nanofluids in Pipes with Different Orientations: A Review.* Journal of Nanofluids, 2017. **6**(6): p. 987-1007.

11. Al-asadi, M.T., et al., *Numerical study of assisting and opposing mixed convective nanofluid flows in an inclined circular pipe.* International Communications in Heat and Mass Transfer, 2017. **85**: p. 81-91.

12. Tuckerman, D.B. and R.F.W. Pease, *High-performance heat sinking for VLSI.* Electron Device Letters, IEEE, 1981. **2**(5): p. 126-129.

13. Dixit, T. and I. Ghosh, *Review of micro- and mini-channel heat sinks and heat exchangers for single phase fluids.* Renewable and Sustainable Energy Reviews, 2015. **41**(0): p. 1298-1311.

14. Mehendale, S.S., A.M. Jacobi, and R.K. Shah, *Fluid Flow and Heat Transfer at Micro- and Meso-Scales With Application to Heat Exchanger Design.* Applied Mechanics Reviews, 2000. **53**(7): p. 175-193.

15. Kandlikar SG, G.W., *Evolution of microchannel flow passages: thermohydraulic performance and fabrication technology.* Proceedings of the ASME international mechanical engineering congress exposition, 2002.

16. Cheraghi, M., M. Raisee, and M. Moghaddami, *Effect of cylinder proximity to the wall on channel flow heat transfer enhancement.* Comptes Rendus Mécanique, 2014. **342**(2): p. 63-72.

17. Albadr, J., S. Tayal, and M. Alasadi, *Heat transfer through heat exchanger using Al2O3 nanofluid at different concentrations.* Case Studies in Thermal Engineering, 2013. **1**(1): p. 38-44.

18. Al-Damook, A., et al., *An experimental and computational investigation of thermal air flows through perforated pin heat sinks.* Applied Thermal Engineering, 2015. **89**: p. 365-376.

19. Manca, O., S. Nardini, and D. Ricci, *A numerical study of nanofluid forced convection in ribbed channels.* Applied Thermal Engineering, 2012. **37**(0): p. 280-292.

20. Ahmed, M.A., et al., *Effect of corrugation profile on the thermal–hydraulic performance of corrugated channels using CuO–water nanofluid.* Case Studies in Thermal Engineering, 2014. **4**(0): p. 65-75.

21. Wang, C.-C. and J.-S. Liaw, *Air-side performance of herringbone wavy fin-and-tube heat exchangers under dehumidifying condition – Data with larger diameter tube.* International Journal of Heat and Mass Transfer, 2012. **55**(11–12): p. 3054-3060.

22. Li, L., et al., *Numerical simulation on flow and heat transfer of fin-and-tube heat exchanger with longitudinal vortex generators.* International Journal of Thermal Sciences, 2015. **92**(0): p. 85-96.

23. Johnson, T. and P. Joubert, *The influence of vortex generators on the drag and heat transfer from a circular cylinder normal to an airstream.* Journal of Heat Transfer, 1969. **91**(1): p. 91-99.

24. Ebrahimi, A., E. Roohi, and S. Kheradmand, *Numerical study of liquid flow and heat transfer in rectangular microchannel with longitudinal vortex generators.* Applied Thermal Engineering, 2015. **78**(0): p. 576-583.

25. Ahmed, H.E., H.A. Mohammed, and M.Z. Yusoff, *An overview on heat transfer augmentation using vortex generators and nanofluids: Approaches and applications.* Renewable and Sustainable Energy Reviews, 2012. **16**(8): p. 5951-5993.

26. Min, C., et al., *Experimental study of rectangular channel with modified rectangular longitudinal vortex generators.* International Journal of Heat and Mass Transfer, 2010. **53**(15–16): p. 3023-3029.

27. Habchi, C., et al., *Enhancing heat transfer in vortex generator-type multifunctional heat exchangers.* Applied Thermal Engineering, 2012. **38**(0): p. 14-25.

28. Kherbeet, A.S., et al., *Mixed convection nanofluid flow over microscale forward-facing step — Effect of inclination and step heights.* International Communications in Heat and Mass Transfer, 2016. **78**: p. 145-154.

29. Kherbeet, A.S., et al., *Heat transfer and fluid flow over microscale backward and forward facing step: A review.* International Communications in Heat and Mass Transfer, 2016. **76**: p. 237-244.

30. Kai-Shing, Y., et al., *On the Heat Transfer Characteristics of Heat Sinks: With and Without Vortex Generators.* Components and Packaging Technologies, IEEE Transactions on, 2010. **33**(2): p. 391-397.

31. Chen, C., et al., *A study on fluid flow and heat transfer in rectangular microchannels with various longitudinal vortex generators.* International Journal of Heat and Mass Transfer, 2014. **69**: p. 203-214.

32. Liu, C., et al., *Experimental investigations on liquid flow and heat transfer in rectangular microchannel with longitudinal vortex generators.* International Journal of Heat and Mass Transfer, 2011. **54**(13–14): p. 3069-3080.

33. Mirzaee, H., et al., *HEAT TRANSFER ENHANCEMENT IN MICROCHANNELS USING AN ELASTIC VORTEX GENERATOR.* 2012. **19**(3): p. 199-211.

34. Leu, J.-S., Y.-H. Wu, and J.-Y. Jang, *Heat transfer and fluid flow analysis in plate-fin and tube heat exchangers with a pair of block shape vortex generators.*

International Journal of Heat and Mass Transfer, 2004. **47**(19–20): p. 4327-4338.

35. Wu, J.M. and W.Q. Tao, *Effect of longitudinal vortex generator on heat transfer in rectangular channels.* Applied Thermal Engineering, 2012. **37**(0): p. 67-72.
36. Khoshvaght-Aliabadi, M., S. Zangouei, and F. Hormozi, *Performance of a plate-fin heat exchanger with vortex-generator channels: 3D-CFD simulation and experimental validation.* International Journal of Thermal Sciences, 2015. **88**(0): p. 180-192.
37. Li, J., et al., *Numerical study on a slit fin-and-tube heat exchanger with longitudinal vortex generators.* International Journal of Heat and Mass Transfer, 2011. **54**(9–10): p. 1743-1751.
38. Chomdee, S. and T. Kiatsiriroat, *Enhancement of air cooling in staggered array of electronic modules by integrating delta winglet vortex generators.* International Communications in Heat and Mass Transfer, 2006. **33**(5): p. 618-626.
39. Ma, J., et al., *Experimental investigations on single-phase heat transfer enhancement with longitudinal vortices in narrow rectangular channel.* Nuclear Engineering and Design, 2010. **240**(1): p. 92-102.
40. Xia, G.D., et al., *Effects of different geometric structures on fluid flow and heat transfer performance in microchannel heat sinks.* International Journal of Heat and Mass Transfer, 2015. **80**(0): p. 439-447.
41. Chai, L., G.D. Xia, and H.S. Wang, *Parametric study on thermal and hydraulic characteristics of laminar flow in microchannel heat sink with fan-shaped ribs on sidewalls – Part 1: Heat transfer.* International Journal of Heat and Mass Transfer, 2016. **97**: p. 1069-1080.
42. Chai, L., G.D. Xia, and H.S. Wang, *Numerical study of laminar flow and heat transfer in microchannel heat sink with offset ribs on sidewalls.* Applied Thermal Engineering, 2016. **92**: p. 32-41.
43. Wang, J. and Y. Zhao, *Heat and fluid flow characteristics of a rectangular channel with a small diameter circular cylinder as vortex generator.* International Journal of Thermal Sciences, 2015. **92**: p. 1-13.
44. Al-Asadi, M.T., F.S. Alkasmoul, and M.C.T. Wilson, *Heat transfer enhancement in a micro-channel cooling system using cylindrical vortex generators.* International Communications in Heat and Mass Transfer, 2016. **74**: p. 40-47.
45. Yu, X., et al., *Development of a plate-pin fin heat sink and its performance comparisons with a plate fin heat sink.* Applied Thermal Engineering, 2005. **25**(2–3): p. 173-182.
46. Jonsson, H. and B. Moshfegh, *Modeling of the thermal and hydraulic performance of plate fin, strip fin, and pin fin heat sinks-influence of flow bypass.* IEEE Transactions on Components and Packaging Technologies, 2001. **24**(2): p. 142-149.
47. Kawano, K., et al., *Micro channel heat exchanger for cooling electrical equipment.* ASME Heat Transfer Div Publ Htd, 1998. **361**: p. 173-180.

48. Qu, W. and I. Mudawar, *Analysis of three-dimensional heat transfer in micro-channel heat sinks.* International Journal of Heat and Mass Transfer, 2002. **45**(19): p. 3973-3985.

49. Gurrum, S.P., et al., *Thermal issues in next-generation integrated circuits.* Device and Materials Reliability, IEEE Transactions on, 2004. **4**(4): p. 709-714.

50. Yuan, W., et al., *Numerical simulation of the thermal hydraulic performance of a plate pin fin heat sink.* Applied Thermal Engineering, 2012. **48**(0): p. 81-88.

51. Promvonge, P., S. Sripattanapipat, and S. Kwankaomeng, *Laminar periodic flow and heat transfer in square channel with 45° inline baffles on two opposite walls.* International Journal of Thermal Sciences, 2010. **49**(6): p. 963-975.

Table captions

Table 1: Micro-channel and VGs dimensions in µm

Micro-channel dimensions (µm)							
H_c	700	**H_t**	900	**W_c**	500	**w_w**	300
VGs dimensions (µm)							
Triangle		**Rectangle**		**Rectangular**		**Circle**	
h	300	**h**	315	**h=b**	250.6628	**r**	200
b	418.879	**b**	200				

Table 2: The boundary conditions of the conjugate heat transfer model.

Locations	Fluid Conditions	Thermal Conditions	Locations	Fluid Conditions	Thermal Conditions
Inlet	50≤ Re ≤2300	T_f=293.15K	**Bottom wall of microchannel**	$\dot{m} = 0$	q=100W/cm^2 constant
Right and left sides (symmetry)	$\frac{du}{dy} = 0$	$\frac{dT}{dy} = 0$	**Pressure outlet**	P=0	$\frac{dT}{dx} = 0$
Top wall and other walls	$\dot{m} = 0$	$\frac{dT}{dz} = 0$	**Microchannel heat sink**	$\dot{m} = 0$	$k_{air}\frac{dT_{air}}{dn} = k_S.\frac{dT_S}{dn}$

Figure captions

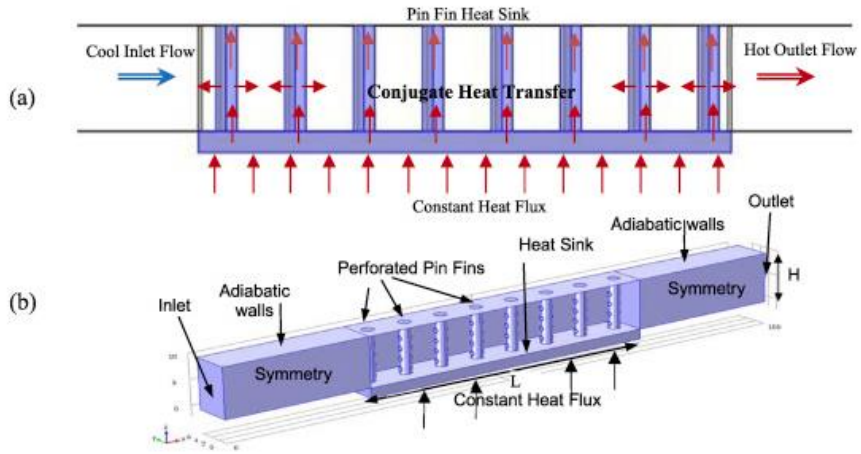

Figure 1: PPHS model description, (a) pinned heat sink; (b) boundary condition of perforated pinned heat sink [17].

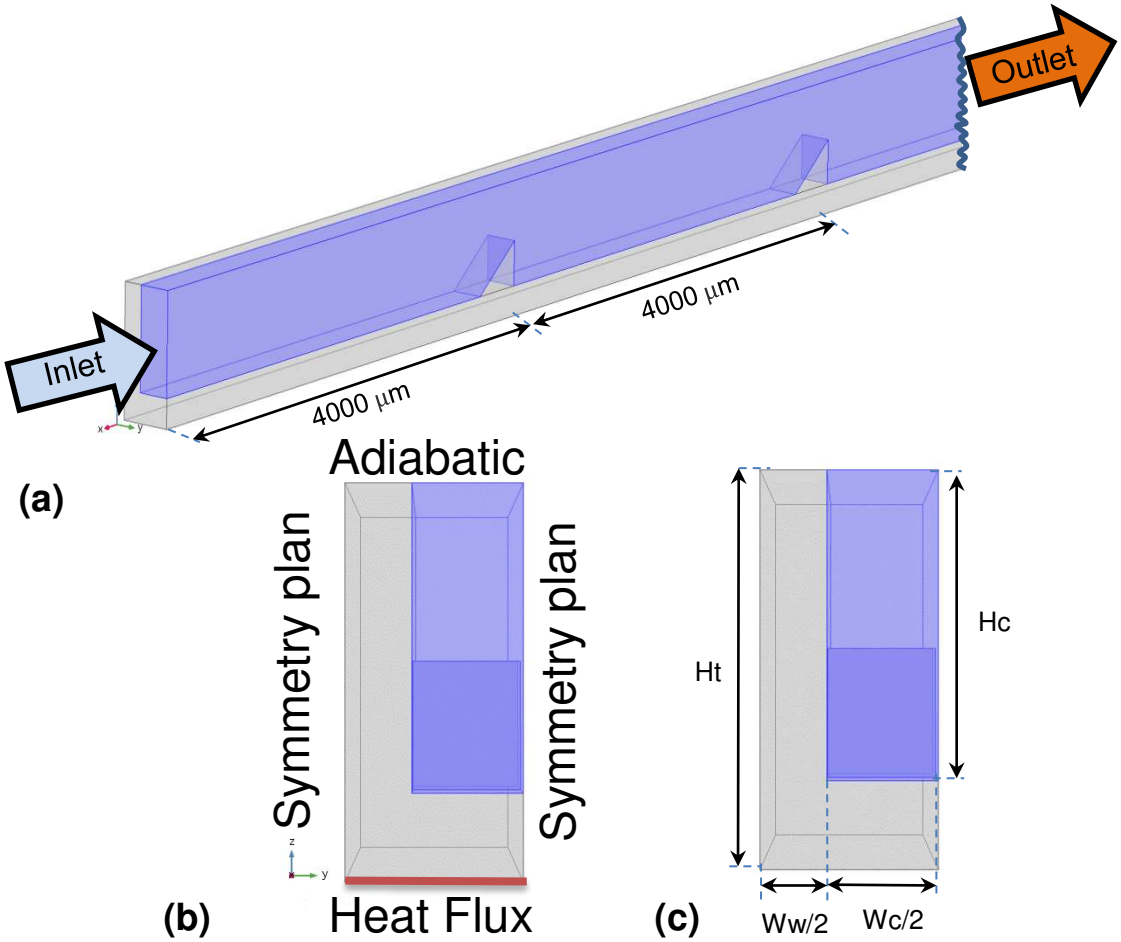

Figure 2: Geometry description: (a) rectangular micro-channel containing vortex generators; (b) boundary conditions of the micro-channel; (c) view along the channel showing the definition of parameters governing the dimensions of the geometry.

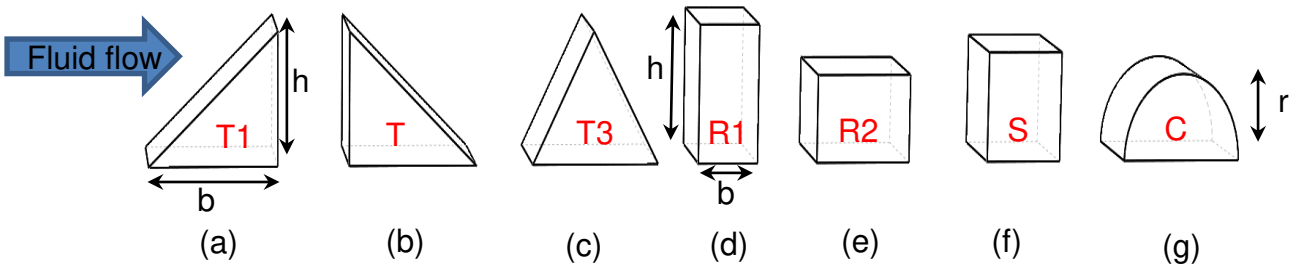

Figure 3: Side view of different shapes of VGs: (a) Forward triangular (T1); (b) Backward triangular (T); (c) Symmetry triangular (T3); (d) Vertical rectangular (R1); (e) Horizontal rectangular (R2); (e) Square (S); (c) Half-circle (C).

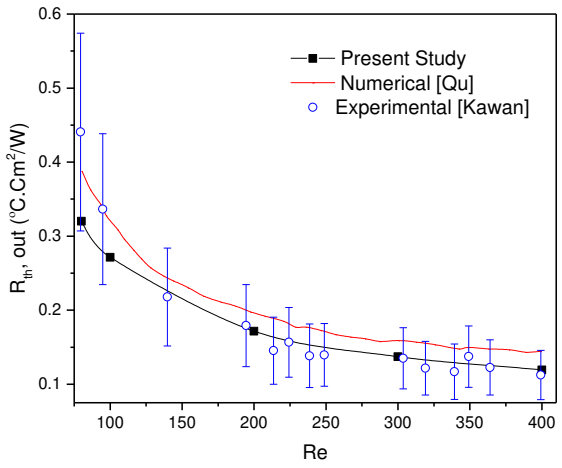

Figure 4: Validation of the present model against experimental data of Kawano *et al.* [47] and alternative numerical results of Qu and Mudawar [48].

.

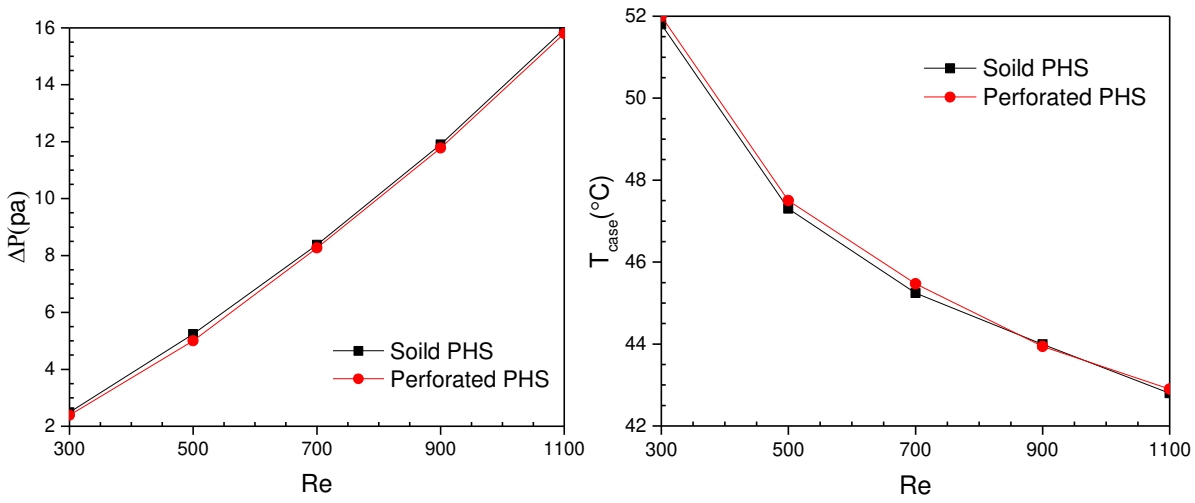

(a) (b)

Figure 5: Comparisons between solid and perforated PHS (3 holes) with water as a coolant: (a) Pressure drop; (b) Base plate temperature.

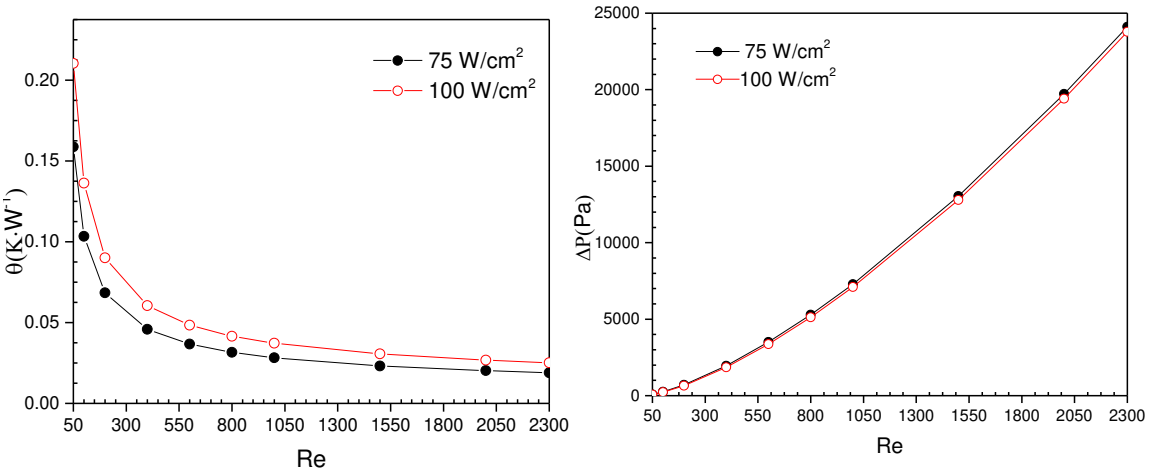

(a) (b)

Figure 6: Different range of heat flux with the full range of Re using uniform channel: (a) thermal resistance; (b) pressure drop.

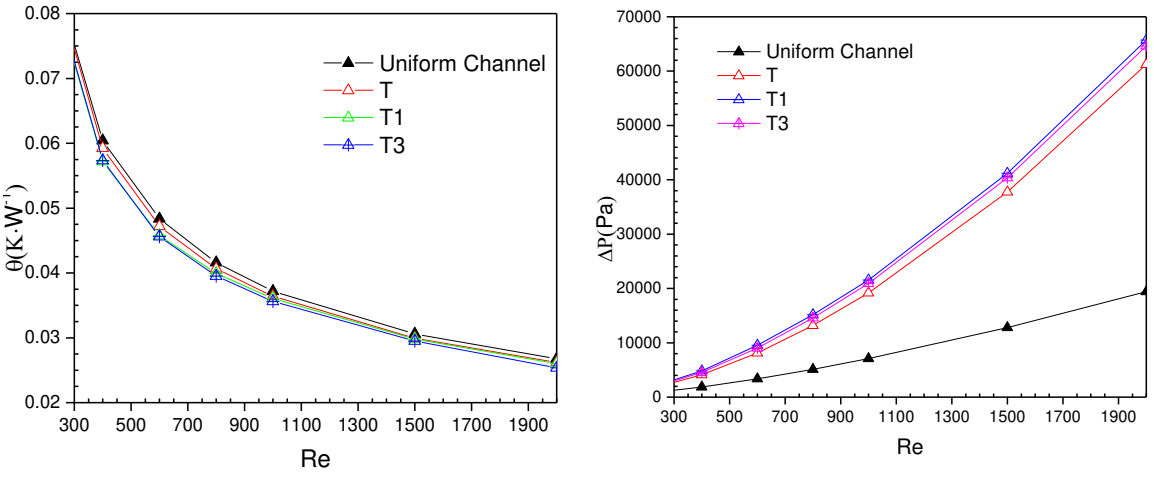

(a) **(b)**

Figure 7: Different configurations of triangular VGs forward triangular (T1), backward triangular (T) and Symmetric triangular (T3): (a) thermal resistance; (b) pressure drop.

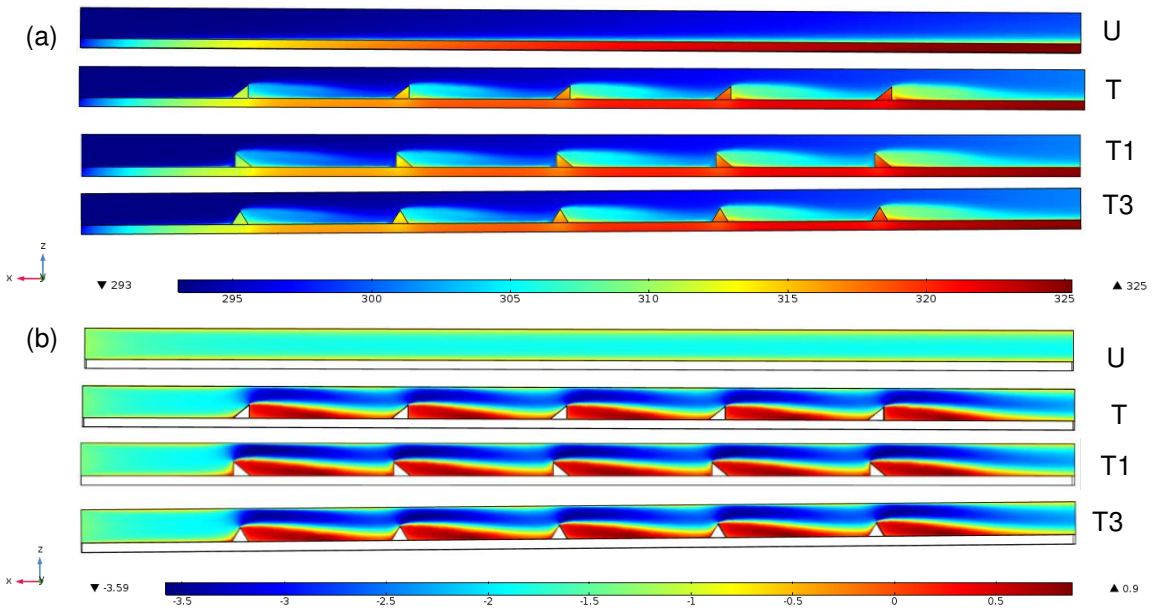

Figure 8: X-Z planes of various triangular VGs models with flow direction from the right to the left at Re 800: (a) temperature contour (K) at the wall of the channel; (b) velocity contour (m/s) at the centre of the channel (400 µm).

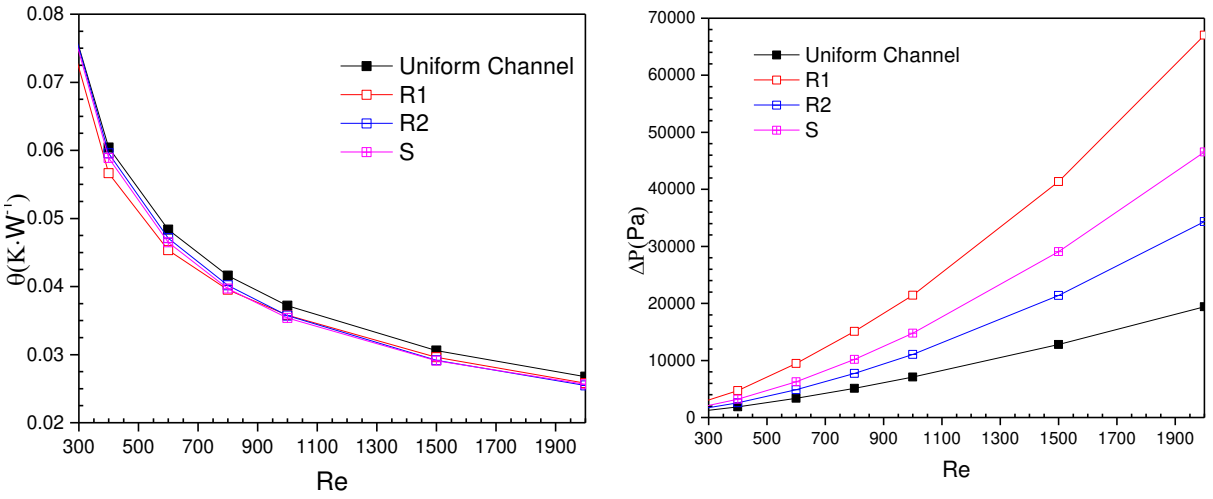

(a) **(b)**

Figure 9: different VGs of rectangular model (Vertical rectangular (R1), Horizontal rectangular (R2) and Square (S)): (a) thermal resistance; (b) pressure drop.

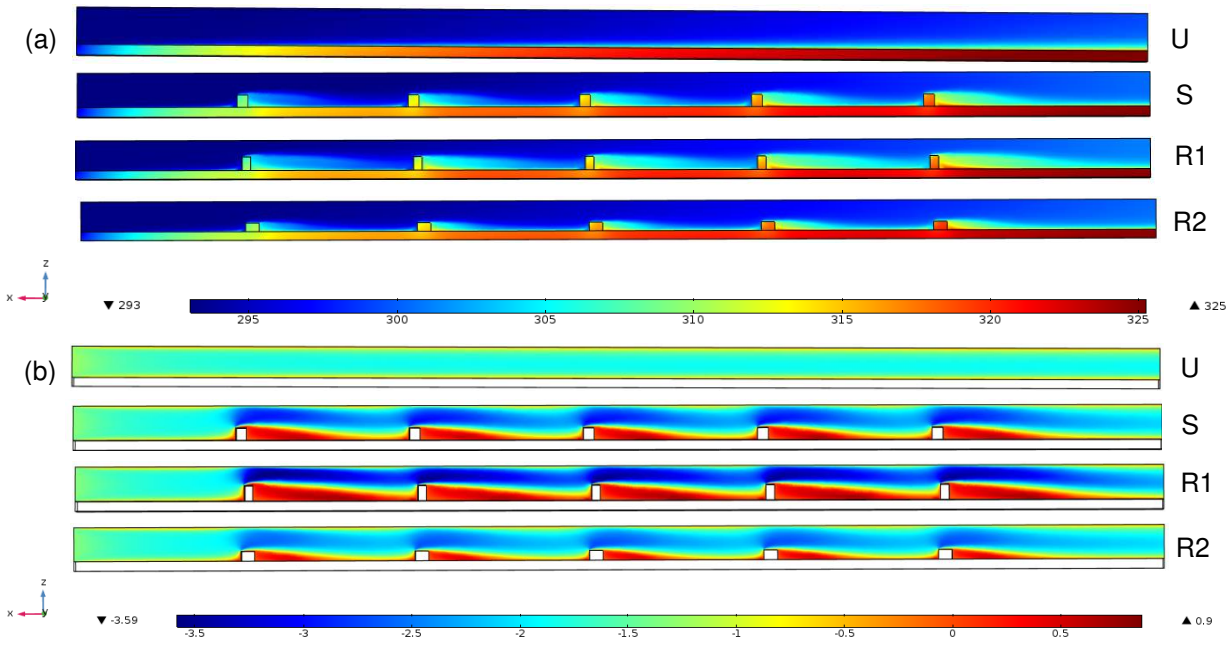

Figure 10: X-Z planes of various triangular VGs models (Vertical rectangular (R1), Horizontal rectangular (R2) and Square (S)) with flow direction from the right to the left at Re 800: (a) temperature contour (K) at the wall of the channel; (b) velocity contour (m/s) at the centre of the channel (400 µm).

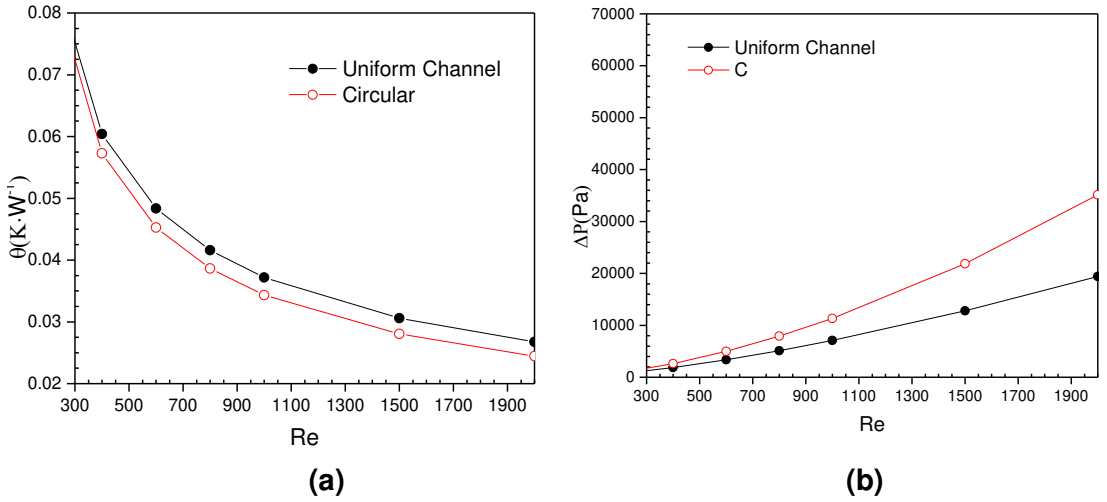

Figure 11: Circular VGs compared to uniform channel using Re from 300 to 2000: (a) thermal resistance; (b) pressure drop.

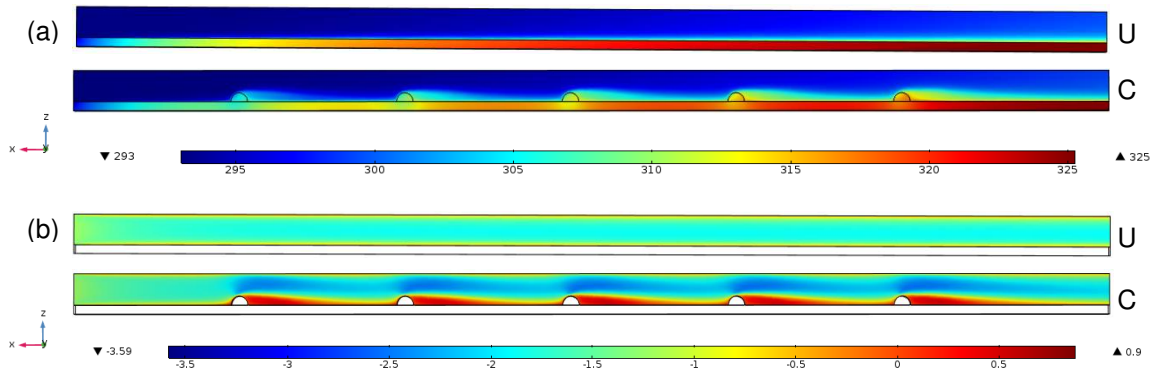

Figure 12: x-z plan of uniform channel and circular VGs at Re =800: (a) temperature contour; (b) velocity contour.

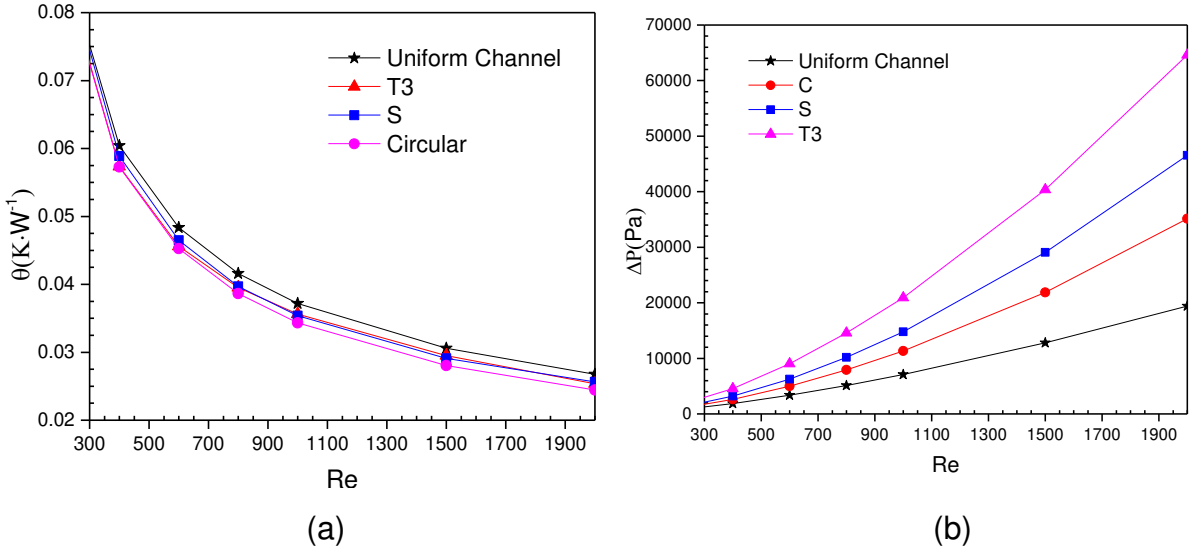

Figure 13: Comparison of the lowest thermal resistance configurations (T3, S and C models); (a) thermal resistance; (b) pressure drop.

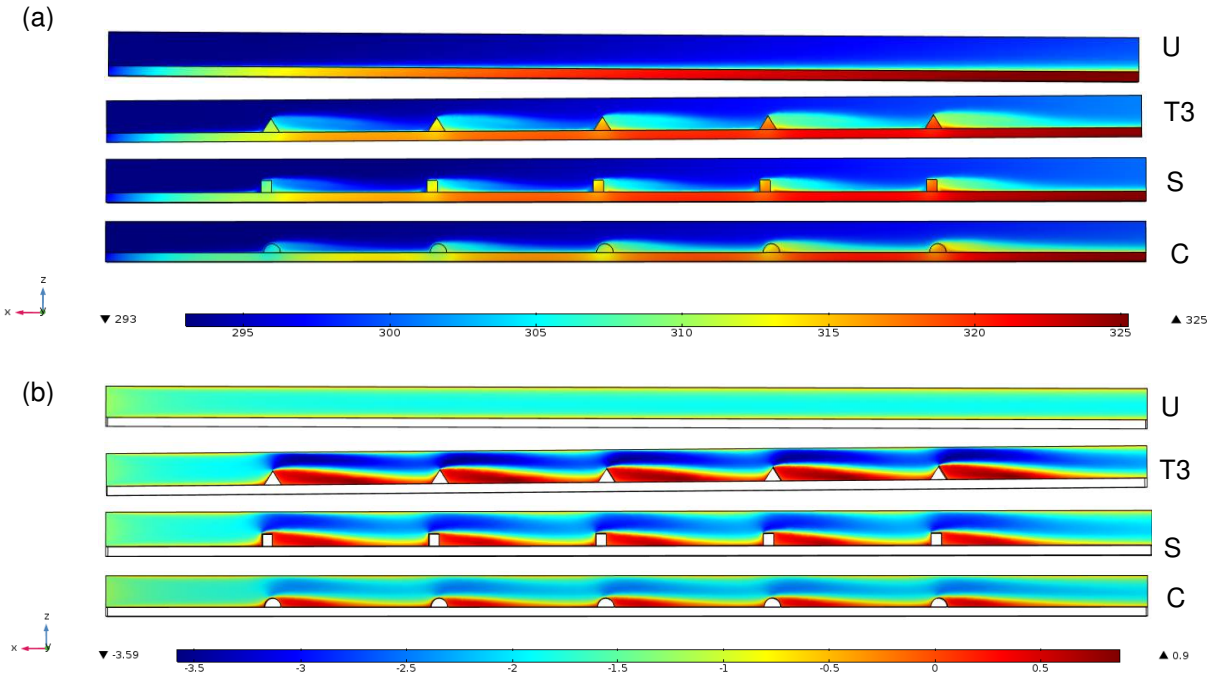

Figure 14: x-z plan comparing the uniform channel to T3, S and C VGs models at Re =800: (a) temperature contour; (b) velocity contour.

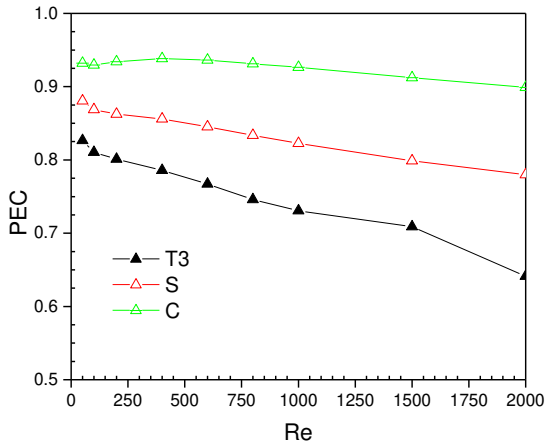

Figure 15: PEC of the lowest thermal resistance models with the full range of Re.